

Some kinetic and synergistic considerations on the oxidation of the azo compound Ponceau 4R by solar-mediated heterogeneous photocatalytic ozonation

Diego H. Quiñones-Murillo*, Angélica A. Ariza-Reyes, Luis J. Ardila-Vélez

Grupo de Procesos Químicos y Bioquímicos Sostenibles, Facultad de Ingeniería, Universidad del Atlántico, 081007 Puerto Colombia, Colombia, Tel. +57-5-3852266 Ext. 1121; emails: diegoquinones@mail.uniatlantico.edu.co (D.H. Quiñones-Murillo), aariza@mail.uniatlantico.edu.co (A.A. Ariza-Reyes), ljardila@mail.uniatlantico.edu.co (L.J. Ardila-Vélez)

Received 31 March 2019; Accepted 22 July 2019

ABSTRACT

A series of advanced oxidation processes were applied to degrade a typical pollutant of industrial effluents known as Ponceau 4R. For this, a magnetic Fenton catalyst was prepared by co-precipitation of Fe^{2+} and Fe^{3+} ions over activated carbon. This catalyst was characterized by XRD, FTIR, VSM and applied in oxidation processes involving the use of ozone, hydrogen peroxide and solar light. Experiments were carried out at laboratory scale in a semi-continuous reactor loaded with a solution of 50 mg L^{-1} of Ponceau 4R in different water matrices (deionized water, domestic wastewater and seawater) and bubbled with air or an ozone–air mixture. When used, the initial concentration of H_2O_2 was $3.3 \times 10^{-2} \text{ mol L}^{-1}$ and that of the catalyst was 500 mg L^{-1} . Results show that Ponceau 4R does not photolyze under solar radiation, it is not directly oxidized by H_2O_2 (in the dark) but it can be partially or entirely degraded through photo-Fenton and ozone-based oxidation processes. Taking into account the initial depletion rate of azo groups concentration and colour removal yield, the efficiency of the tested systems follows the order: hydrogen peroxide photolysis < photo-Fenton process < perozone < ozonation < catalytic ozonation \approx photocatalytic ozonation. Ponceau 4R was also completely removed from real domestic wastewater and seawater samples, which were doped with this compound and subjected to photocatalytic ozonation treatment, in less than 60 min of reaction time, when the matrices pH was previously adjusted to 3. However, when applied at the natural pH of these water matrices (8 and 8.7, respectively), the pollutant conversion was 80%.

Keywords: Advanced oxidation processes; Magnetic catalyst; Ponceau 4R; Solar photocatalytic ozonation; Synergistic effect

1. Introduction

The annual global consumption of azo compounds in the chemical process industry is estimated to be over 700,000 tons [1]. The chemical structure of an azo compound is characterized by the presence of at least one azo functional group that consists of a pair of nitrogen atoms linked to each other by a double bond, both sp^2 hybridized and bonded to aryl or alkylic carbon chains [2]. The use of this type of chemical substances has been many times questioned because they are recalcitrant to conventional

water treatment methods and some have been identified as carcinogenic and teratogenic agents, precisely because of the presence of the azo bond [1].

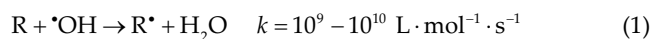
Azo compound Ponceau 4R (CASRN 2611-82-7), also known as cochineal red A, E124 or acid red 18 among others names, is a red colouring powder widely used to impart scarlet red tonalities in textile, food, pharmaceutical and toiletry products [3–5]. This additive is being subjected to investigation since it is suspected to trigger hyperactivity disorders in children, affect infants' brain development, provoke allergic reactions, asthma, rhinitis, urticaria and cause tumours in animals [6–9]. And although it has been

* Corresponding author.

banned in countries such as United States, Canada, Finland and Norway, it is still authorized in many other countries. Table 1 summarizes some physicochemical characteristics of Ponceau 4R.

Since many synthetic dyes such as Ponceau 4R are largely used in many industrial processes, they have become common wastewater pollutants [10]. Their negative effects on aquatic environments include the blocking or reduction of light penetration into the water that affects biological processes as photosynthesis, reduces the oxygen diffusion and causes eutrophication problems [11]. This type of substances is usually characterized by a high water solubility and chemical stability, and therefore they are classified as recalcitrant water pollutants that need advanced treatments to be removed from the environment.

In this study, a series of advanced oxidation processes (AOPs) were applied to treat surface water samples spiked with Ponceau 4R dye. AOPs are physicochemical processes that consist in the generation of highly reactive short-lived oxygen species, particularly the hydroxyl radical ($\cdot\text{OH}$) that reacts in a nonselective way with organic pollutants at rate constants ranging between 10^9 and 10^{10} $\text{L mol}^{-1} \text{s}^{-1}$ [12,13]. This reactivity is due to the presence of one unpaired electron in its structure, so it tends to oxidize other molecules by capturing an electron from them Eq. (1).



R represents the organic contaminant and R^{\cdot} is the contaminant once oxidized. If generated in sufficient concentration, $\cdot\text{OH}$ radicals can achieve complete degradation and mineralization of organic compounds to CO_2 , H_2O and

mineral acids. Hydroxyl radical can be generated by the combination of oxidizing agents such as hydrogen peroxide or ozone, catalytic materials (e.g., iron ions and semiconductors) and irradiation (e.g., ultraviolet and solar light) [14]. The AOPs studied in this work are listed in Table 2.

Hydrogen peroxide photolysis consists in the homolytic cleavage of the HO–OH bond into $\cdot\text{OH}$ under UV radiation (Eq. (2)), which is effective under radiation of wavelengths shorter than 380 nm [15]. However, an important limiting factor of this process is the efficiency of energy absorption of H_2O_2 to produce $\cdot\text{OH}$, since it drastically changes with wavelength. For instance, H_2O_2 molar absorption coefficient vary from $180 \text{ L mol}^{-1} \text{ cm}^{-1}$ at wavelengths in the range 200–204 nm, to about $19.6 \text{ L mol}^{-1} \text{ cm}^{-1}$ at 254 nm, and to $0.88 \text{ L mol}^{-1} \text{ cm}^{-1}$ close to 300 nm [16].



Hydrogen peroxide also decomposes into reactive oxygen species in the presence of ferrous ion in a complex mechanism initiated by the so-called Fenton reaction Eq. (3), which is followed by Eq. (4) where formed Fe^{3+} reacts with H_2O_2 to regenerate Fe^{2+} (referred to as Fenton-like reaction) [17]. Many other reactions occur simultaneously in the process to give different reactive oxygen species, but the most relevant are presented below.

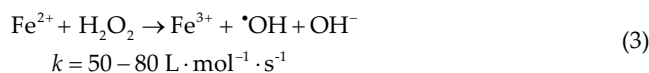
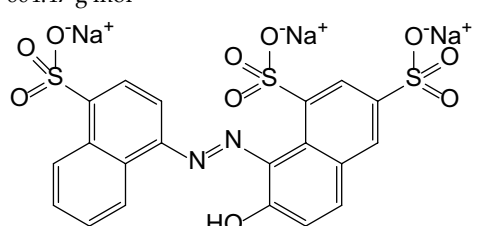


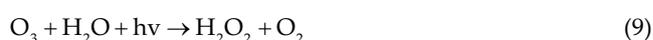
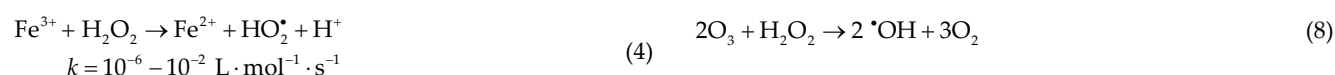
Table 1
Physicochemical properties of Ponceau 4R dye

| Property | Value |
|---|--|
| Molecular formula | $\text{C}_{20}\text{H}_{11}\text{N}_2\text{Na}_3\text{O}_{10}\text{S}_3$ |
| Molar mass | $604.47 \text{ g mol}^{-1}$ |
| Chemical structure |  |
| Dissociation constant values (pK) | $-\text{SO}_3\text{H}$ groups: -0.6, 0.4 and 0.9 $-\text{N}=\text{N}-$: 2.7 $-\text{OH}$: 11.5 [4] |
| Wavelength of maximum absorbance and molar absorptivity | 508 nm^a ; $2.066 \times 10^{-2} \text{ L mol}^{-1} \text{ cm}^{-1}$ [5] |
| Solubility | Water: 80 mg mL^{-1} Ethanol: 0.9 mg mL^{-1} [9] |
| Vapor pressure | $1.3 \times 10^{-27} \text{ mmHg}$ at 25°C [9] |
| Acceptable daily intake | JECFA: 4 mg kg^{-1} (mg per kg body weight) EFSA: 0.7 mg kg^{-1} [8] |

^aPonceau 4R UV-visible absorption spectra is shown in Fig. S1.

Table 2
AOPs applied in this work

| AOP | Oxidizing agents | Abbreviation |
|------------------------------|---|--------------|
| Hydrogen peroxide photolysis | H ₂ O ₂ + UV light | HPP |
| Photo-Fenton-like process | H ₂ O ₂ + iron source + UV light | PFP |
| Peroxone | H ₂ O ₂ + O ₃ | PER |
| Single ozonation | O ₃ | OZO |
| Catalytic ozonation | O ₃ + iron source + H ₂ O ₂ | COZH |
| Photocatalytic ozonation | O ₃ + iron source + UV light + H ₂ O ₂ | PCOH |



The regeneration of ferrous iron through Eq. (4) is a limiting stage of the Fenton process given its low reaction constant; however, the use of radiation can increase the global reaction rate [18]. When Fenton reaction is carried out under radiation, the process is known as photo-Fenton and the production of $\cdot\text{OH}$ is enhanced since, in addition to the reactions described by Eqs. (2)–(4), in the system also occurs the photolysis of hydroxycomplexes formed between Fe^{3+} and water, which are stable in the dark. This reaction that can happen under UV radiation, represents an alternative way to regenerate Fe^{2+} (Eq. (5)) [17,19].



A limiting factor of Fenton systems is their narrow pH of application, which is in the range of 2.8–3.0. At lower pH values, the production of $\cdot\text{OH}$ radicals is reduced, while at higher pH, $\cdot\text{OH}$ radicals are scavenged by H^+ and additionally, iron solubility is severely reduced and precipitates in the form of oxyhydroxide species [20,21]. Another drawback is the formation of iron sludge and the need of recovering the catalyst after treatment. However, the use of easily separable iron-based solid catalysts leads to the possibility of performing heterogeneous Fenton reactions [17]. Iron-containing materials are sources of continuous dissolution of iron and allow the process to be operated at mild pH conditions avoiding the addition of extra ions to acidify the oxidation medium [22,23].

Ozonation systems can indirectly oxidize organic compounds by the generation of hydroxyl radicals from the ozone depletion in water. This process can be accelerated by the presence of iron (in catalytic ozonation Eqs. (6) and (7) [24]), H₂O₂ (in peroxone process Eq. (8) [25]) or UV radiation (in photolytic ozonation Eq. (9) followed by Eq. (2)) [26]. Additionally, ozone can directly attack unsaturated linkages and certain moieties (amines, carboxylic acids, ketones, etc.) present on the organic contaminants structure [19,27].



Photocatalytic ozonation represents the combination of all mechanisms above presented. Therefore, in this system the target contaminant is simultaneously degraded by direct and indirect reaction with ozone, and oxidation by the $\cdot\text{OH}$ generated through photocatalysis or H₂O₂ photolysis, if present. Other parallel events that can take place in this process are the partial adsorption of the contaminants on the catalyst surface and their direct photolysis. The combination of these mechanisms results in an important synergistic effect [28].

As one of the main disadvantages of AOPs is the need of recovering the catalysts from the reaction medium at the end of the process, the preparation of a magnetically separable catalyst is presented in this study as an alternative to reduce operational costs by its recycling in catalytic AOPs. This material was tested in the degradation of Ponceau 4R, chosen as model compound of azo dyes, typical contaminants of polluted surface waters. This catalyst, besides being useful in Fenton-like processes, was able to absorb contaminant particles from water through its activated carbon support.

As the type of water matrix can strongly impact the efficacy of these AOPs, since some water constituents can absorb radiation, precipitate iron ions in the form of insoluble salts and/or scavenge hydroxyl radicals and other oxygen reactive species [29], in this study we evaluated the use of domestic wastewater and seawater, which are very different in composition and characteristics, as water matrices to study the degradation of the target pollutant. Domestic wastewaters usually have high content of organic matter and some inorganic carbon compounds that compete against the target pollutants for $\cdot\text{OH}$ [30]; while seawater has an important content of ionic species and salinity that may alter the surface properties of a catalysts if used, form insoluble compounds with iron ions during Fenton treatment and scavenge hydroxyl radicals [31,32]. Although wastewater is a well-known source of emerging pollutants; recently, several studies have highlighted the occurrence of contaminants of emerging concern in other water systems such as estuaries, the open sea and coastal waterbodies [33–35]. This represents a risk for marine biota and human consumers of seafood and desalinated water. Thus, the application of AOPs could be considered as an additional stage in the treatment of sweater to produce drinking water.

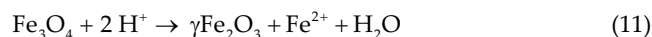
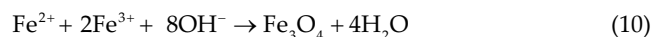
2. Materials and methods

2.1. Reagents

Deionized water was obtained from a Micromatic water purification unit (Wasserlab, Spain). $\text{FeSO}_4 \cdot 7\text{H}_2\text{O}$, $\text{FeCl}_3 \cdot 6\text{H}_2\text{O}$, HCl (37%w/w), NH_4OH (25%w/w), anhydrous ethanol, H_2O_2 (30%w/w), NaOH and activated charcoal GR were purchased from Merck (Germany) and used as received. KBr was purchased from Sharlau Chemie (Spain).

2.2. Catalyst preparation

Magnetic catalyst was prepared by the co-precipitation technique according to the protocol described by Fayazi et al. [36]. Typically, two precursor (Fe^{2+} and Fe^{3+}) solutions were prepared by, respectively, dissolving 5.6 g $\text{FeSO}_4 \cdot 7\text{H}_2\text{O}$ and 10.8 g $\text{FeCl}_3 \cdot 6\text{H}_2\text{O}$ in two separated beakers, each containing 50 mL HCl solution (2 mol L^{-1}). Then, 2.1 g of activated charcoal GR were dispersed into the Fe^{3+} solution under vigorous stirring for 10 min. After that, the Fe^{2+} solution was added and the mixing was kept for a further 10 min, thus a mixture with stoichiometric $\text{Fe}^{3+}:\text{Fe}^{2+}$ molar ratio of 2:1 was obtained. Then, the pH of the mixture was adjusted in the range of 10–11 by adding dropwise a solution of NH_4OH (4 mol L^{-1}). This mixture was kept vigorously stirred for 120 min at room temperature. During this ageing stage, Fe_3O_4 is formed and subsequently transformed into $\gamma\text{Fe}_2\text{O}_3$ according to Eqs. (10) and (11) [37], and deposited on the activated carbon surface.



The so-obtained magnetic activated carbon was magnetically separated from the solution, and rinsed several times using an equivolumetric mixture of ethanol and deionized water. Finally, it was dried at 60°C overnight, manually grinded, screened through a 30-mesh sieve and stored until use.

2.3. Catalysts characterization

Catalyst functional groups were analyzed by Fourier-transform infrared light spectrophotometry in a Shimadzu IR Affinity-1 spectrometer (Japan) at 21°C using KBr wafers containing about 10% w/w of sample. Data were acquired in a wavelength range from 400 to 4,000 cm^{-1} .

X-ray diffraction analysis of the catalyst was performed in a PANalytical Empyrean diffractometer (2012) to identify the crystalline phases of iron oxides present in the catalyst. Diffractograms were recorded over a range of $5^\circ \leq 2\theta \leq 80^\circ$ with a step size of 0.026°s⁻¹. The HighScore Plus suite was used to semi-quantify the content of iron oxides phases by the Rietveld method.

Magnetic properties of the catalyst were analyzed on a vibrating sample magnetometer (VSM 7400 Lake Shore, United States) at 25°C, applying a field between –15 and 15 kOe.

The point of zero charge (pH_{zpc}) for the catalyst was determined according to the pH drift method described by

Babić et al. [38]. The tests were performed using an orbital shaker (HS120460, Heathrow Scientific, United States) using solutions containing 0.3% w/v catalyst and 0.01 mol L^{-1} NaCl at 200 rpm and 20°C, during 48 h of shaking.

2.4. Experimental procedure for the oxidation processes

Experiments were carried out at laboratory scale using a Pyrex-Glass® cylindrical reactor (total capacity of 1 L and 10 cm diameter) operating in semi-continuous mode at ambient temperature, placed on a magnetic stirring plate, and provided with a magnetic stirring bar and a digital thermometer. A portable UV radiometer (PCE-UV34, PCE Instruments, Spain) was used to record the UVA and UVB incident radiation with wavelengths between 290 and 390 nm. Depending on the experiment performed, the reactor was fed with either air or an air-ozone mixture, for this a portable ozone generator (FM-500 CE, Beyok ozone, China) was used for the production of an air–ozone mixture (200 mg h^{-1} O_3), otherwise an air pump was used to bubble air to the reactor. In all cases, gas was continuously fed into the reactor through a porous gas diffuser. Experiments were performed under sunlight in the city Puerto Colombia, in northern Colombia (coordinates: 11° 1' 11.7012'' N, 74° 52' 17.8716'' W).

In a typical experiment, the reactor was first loaded with 500 mL of a Ponceau 4R solution (50 mg L^{-1}). Then, the stirring speed was set to 1,500 rpm and if required, the pH of the solution was adjusted to the desired value by adding either dilute NaOH or dilute HCl . After that, the reactor was simultaneously uncovered and placed under sunlight for the photochemical systems, added with H_2O_2 or catalyst if needed, and fed with the gas mixture. This time was considered as the zero time.

To monitor the extent of dye removal, the decrease of absorbance of the solution at 508 nm was measured in an UV-Visible spectrophotometer (Evolution™ 60S, Thermo Fisher, United States) from reaction samples taken at regular time interval during 90 min. Chromophore concentration in each reaction sample was estimated spectrophotometrically from the solution absorbance at 508 nm and using the Beer-Lambert law. Hydrogen peroxide concentration was measured using the Masschelein method [39].

These experiments were conducted using different water matrices such as deionized water, real domestic wastewater or natural seawater. The domestic wastewater sample was collected from the effluent of a biological treatment plant that treats the sewage generated by the Universidad del Atlántico's population (ca. 24,000 people). Seawater was taken from Santa Verónica beach on the Caribbean coast of Colombia (coordinates 10°52'37''N, 75°5'3''W). Both samples were collected by single sampling, doped with the target azo compound without any additional modification and subjected to treatment, at their natural pH and a pH of 3, to estimate how their properties affect the efficiency of the oxidation processes.

Standard methods were used to determine total solids content (method 2540B) and chemical oxygen demand (method 5220D) of the water [40]. Water conductivity was measured in an RS Pro conductivity meter (model 180-7127). Water turbidity was measured in an ISO portable

turbidimeter (98713, Hanna Instruments, United States). Measurements of pH were carried out using an Orion pH meter (210A+, Thermo Electron Corporation, United States).

3. Results and discussion

3.1. Catalyst characterization

Fig. 1 shows the XRD patterns of the catalyst that confirms the presence of magnetite and maghemite as the only phases of iron oxide obtained in the catalyst. This pattern corresponds to a cubic structure, which is ascribed to both magnetite and maghemite whose Bragg reflection peaks are very close. The diffraction peaks identified for both phases correspond to the lattices denoted by miller indices hkl , (311), (400), (422), (440) and (533). In addition, two characteristic peaks for maghemite, (210) and (211), were appreciable [41]. The (311), (400) and (422) peaks were used to calculate the average crystallite size for the iron oxides through the Scherrer equation and was found to be 25.67 nm. Carbon peaks for (002) and (101) lattices were also identified, the latter overlapping with that of the (400) lattice for the iron oxides. This diffractogram was analyzed by the Rietveld refinement technique in order to semi-quantify the magnetite/maghemite mass ratio which resulted to be 3.41.

The FTIR spectra for the catalyst are shown in Fig. 2. The sharp peaks identified at 3,475 and 3,414 cm^{-1} correspond to the stretching vibration mode of primary amines, also a shoulder band is noted at 3,259 cm^{-1} , which is an overtone of the N–H bending vibration. The small bands at 2,922 and 2,902 cm^{-1} are due to the symmetric and asymmetric stretching of aliphatic C–H. The sharp peak at 2,360 cm^{-1} is ascribed to the asymmetric stretching of CO_2 adsorbed on the catalyst. The weak band at 2,070 cm^{-1} corresponds to the stretching vibration in alkyne groups. The absorption band at 1,745 cm^{-1} is related to C=O stretching vibration. At 1,635 cm^{-1} a peak is present due to N–H bending vibration. The band at 1,550 cm^{-1} can be related to stretching of aromatic C=C bonds. The band at 1,153 cm^{-1} is characteristic of C–O structures from phenolic hydroxyl, aromatic ethers

or carboxylic acids. Finally, the peak at 640 is due to Fe–O bending [42,43].

Fig. 3 corresponds to the determination of the catalyst pH_{zc} by the pH drift method, which turned out to be 6.95. This value represents the pH of the medium at which the catalyst surface has a net neutral charge. When the catalyst is dispersed in a solution under a pH below its pH_{zc} , the catalyst surface is positively charged and consequently it tends to attract negative ions by electrostatic attraction. In contrast, the adsorption of positive ions is favoured at pH above the catalyst pH_{zc} when its surface is negatively charged.

Fig. 4 shows the magnetic hysteresis loop for the catalyst, which has the typical S-shape of magnetic materials. This narrow loop indicates that the catalyst is a soft ferromagnetic material, so it can be easily magnetized and demagnetized. From the hysteresis loop is calculated a residual magnetism

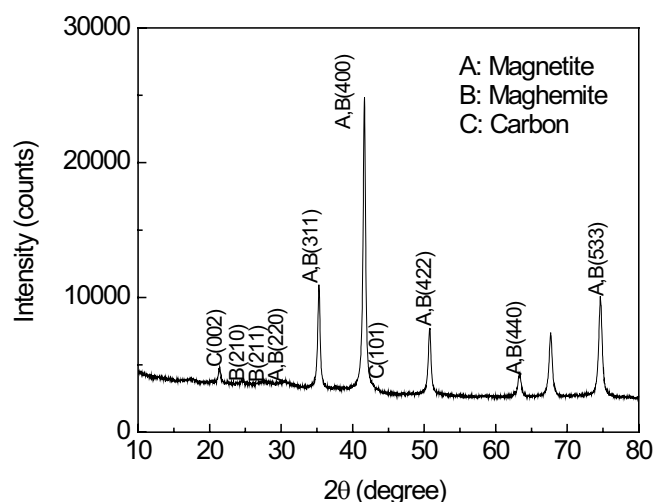


Fig. 1. X-ray diffraction patterns of the catalyst.

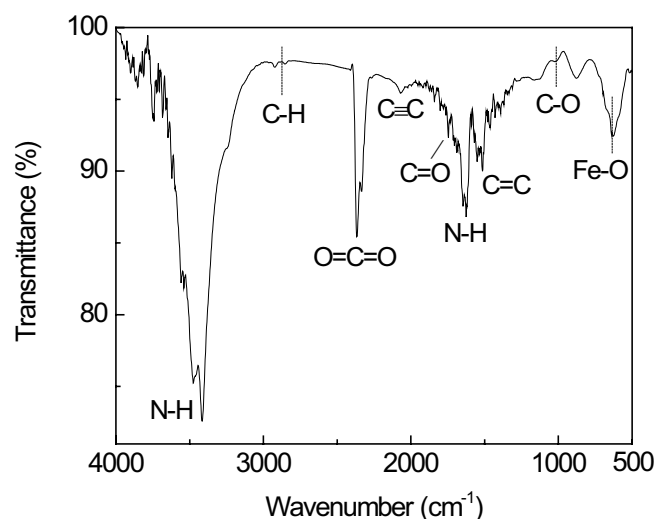


Fig. 2. FTIR spectra of the magnetic catalyst.

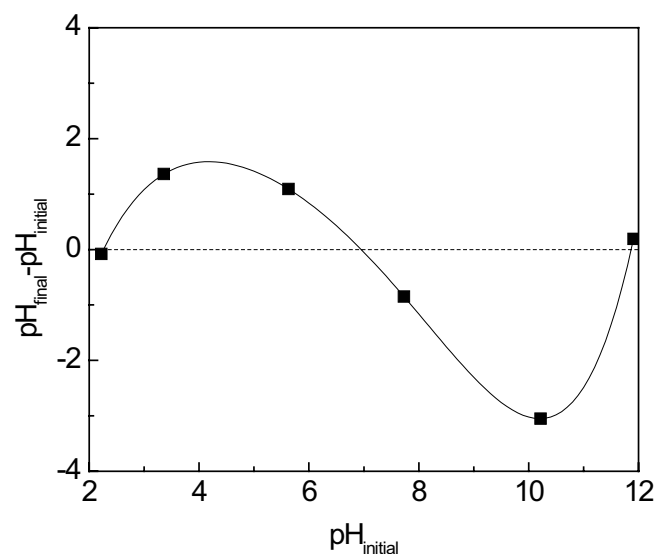


Fig. 3. Determination of the catalyst point of zero charge by the pH drift method.

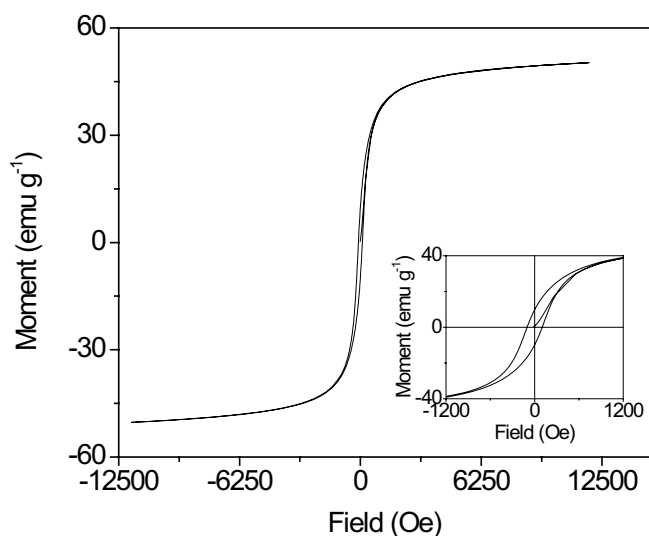


Fig. 4. Magnetic hysteresis loops obtained for the catalyst at 290 K and zoomed-in graph (embedded) for the range from $-1,200$ to $1,200$.

of 9.74 emu g^{-1} , coercive force of 102.01 Oe and saturation magnetization of 38.16 emu g^{-1} . These results indicate that the prepared catalyst effectively shows a sensitive response to an external magnetic field. Due to these magnetic properties, the catalyst particles, when dispersed in water, can be separated by using an external magnet as shown in Fig. S2. These particles do not aggregate after being magnetically separated and can be re-dispersed by stirring once the magnet is moved away.

3.2. Application of treatment processes

3.2.1. Preliminary tests

Some preliminary experiments were carried out to assess the effect of some experimental conditions on the compound stability. First, it was confirmed that Ponceau 4R solutions are stable at room temperature when kept away from light for several months. Ponceau 4R is not volatile in water since it is not removed from the liquid phase when air is sparged through the water at room temperature, nor does it undergoes photolysis under sunlight as no evidence of degradation was observed when subjected to 90 min of solar irradiation (and a total UV light supply of 12.7 kJ L^{-1}). This treatment was extended until reaching 16.7 kJ L^{-1} of UV supply without any improvement in the system performance.

As well, some adsorption primary tests were carried out to evaluate the ability of the synthesized magnetic catalyst to remove the contaminant from water by adsorption. The experiments were performed at pH 5.7 (the natural pH of a 50 mg L^{-1} Ponceau 4R solution in deionized water) and pH 3, accompanied by air bubbling. During these experiments, a 31% of Ponceau 4R was removed after 90 min of treatment. At pH 3 and 5.7, the probe molecule has a net negative charge because of the ionization of its sulfos and azo functional groups (see dissociation constants in Table 1) and the catalyst surface is positively charged

($\text{pH}_{\text{zc}} = 6.95$). Consequently, at both pH, the electrostatic attraction between Ponceau 4R and catalyst is similar and thus no significant changes in the adsorption profiles are expected in this range.

A further adsorption test was carried out in the presence of solar radiation at pH 5.7 in order to assess the catalyst photo-activity under solar radiation. No apparent effect on the dye removal efficiency was observed since a similar removal profile was obtained compared with those of the dark experiments. During this latter adsorption experiment, the total UVA-UVB radiation supplied to the system after 90 min was 12.2 kJ L^{-1} . This is explained by the fact that magnetite has a poor photocatalytic response due to its narrow bandgap (0.14 eV [44]) which leads to recombination of electron-hole pairs when photo-excited; on the other hand, the obtained content of maghemite (whose band gap is 2.3 eV [45]) is not enough to present a significant photocatalytic response and is overshadowed by the adsorption potential of the catalyst.

The adsorption of Ponceau 4R can occur by different mechanisms besides the electrostatic attraction between ionic forms of the probe molecule and the charged groups on the catalyst surface, such as the formation of hydrogen bonds and π -interactions. Hydrogen bonds are formed between hydroxyl group of the dye and oxygen- or nitrogen-containing groups on the catalyst surface (which were identified by the FTIR analysis). Also, the aromatic backbone of the dye molecules can develop π - π stacking interactions with the aromatic structures on the carbon support of the catalyst via face-to-face conformation [46,47]. Additionally, an azo-hydrazone tautomer can be formed due to the proximity of hydroxyl group to the azo group, then the nitrogen atom can form a hydrogen bond with electronegative atoms on the catalyst [48].

3.2.2. AOPs

Solutions of Ponceau 4R dye in deionized water were subjected to a series of AOPs listed in Table 2, wherein the iron source was the magnetic catalyst previously synthesized. Fig. 5 shows the discolouration profiles through the AOPs applied at the natural pH of the solution. For additional information (as the variation of temperature and absorbed UVA-UVB radiation with time throughout the sunlight-mediated experiments), please refer Fig. S3. The discolouration is due to the chromophore cleavage in the target compound by $\cdot\text{OH}$ or O_3 attack and the subsequent molecule degradation into simpler by-products (for a simplified degradation mechanism, Fig. S4).

The combination of H_2O_2 and sunlight in the HPP system led to a synergistic effect; since as previously indicated, no discolouration was observed by solar photolysis or direct H_2O_2 oxidation (in the dark), but the coupling of both agents led to a discolouration percentage of 11% after 90 min of treatment (and 11.1 kJ L^{-1} of UV radiation supplied).

The application of PFP treatment allowed a colour removal yield of 58% (with 10.8 kJ L^{-1} of UV radiation). In this process, a high initial reaction rate was reached ($4.4 \times 10^{-8} \text{ mol L}^{-1} \text{ s}^{-1}$ in terms of azo content removal) but rapidly diminished (falling to $3.7 \times 10^{-9} \text{ mol L}^{-1} \text{ s}^{-1}$ in 10 min)

because of the rapid consumption of added H_2O_2 . A synergistic effect is shown in the PFP system since the reached colour removal yield was higher than the one theoretically expected when summing those individually reached for HPP, direct photolysis and photocatalytic oxidation.

All the ozone-based AOPs led to a complete removal of colour. This is due to the ozone high affinity for chromophoric groups (such as the azo moiety) and aromatic rings as the ones present in Ponceau 4R molecule (Table 1) [49]. Ozone reacts with the probe compound through electrophilic attack of an electron-rich nitrogen atom in the azo functional group or a carbon-carbon double-bond in the aromatic ring [27,50].

PER was the slowest ozone-based AOP, it was less efficient than OZO. This suggests that, under the experimental conditions here applied, the compound depletion occurs mainly by the direct attack of ozone to the probe molecule. The use of H_2O_2 in the dark is expected to lead to the partial depletion of O_3 into radicals [51], but also it is known that H_2O_2 , when used in excess, acts as a scavenger of $\cdot\text{OH}$ [25,52]. Thus, an adverse effect was observed.

The presence of the catalyst in COZH resulted in a high initial degradation rate (around $7.2 \times 10^{-8} \text{ mol L}^{-1} \text{ s}^{-1}$). This is an indicative of a more efficient formation of $\cdot\text{OH}$ compared with HPP or PER. In the COZH process, $\cdot\text{OH}$ generation from ozone depletion is catalyzed by the electrons of the graphenic layers of the carbon support of the catalyst and the presence of basic surface and oxygenated groups or mineral matter such as iron oxides on the surface of the activated carbon [53]. According to the FTIR analysis, the catalyst surface contains oxygenated groups such as C=O and C–O which can suggest the presence of basic groups (such as chromene, pyrone, quinone or diketone groups) and another electron rich ones (such as aromatic C=C). These groups are thought to act as catalytic centers to reduce the

ozone molecule to $\cdot\text{OH}$ radicals or H_2O_2 and improve the system efficiency [54].

The presence of radiation in PCO and PCOH also led to one of the highest initial reaction rates and fastest colour removal reached in this study. This is due to a synergistic effect that improves the $\cdot\text{OH}$ generation. In these systems, several mechanisms to generate $\cdot\text{OH}$ radicals come together: H_2O_2 photolysis, O_3 photolysis, Fenton-like process, O_3 catalytic degradation and O_3 depletion in water.

3.2.3. Influence of the pH

Since pH is a crucial factor in the efficiency of Fenton-catalyzed oxidation processes, some selected systems were also applied at pH 3 to evaluate the effect of this factor on the efficiency of these treatments. Fig. 6 shows the colour removal profiles obtained at pH 3. As a general trend, the AOP systems applied showed better performance when applied at pH 3 than at pH 5.7. Fig. 7 displays a comparison for the initial degradation rates obtained at pH 3 and 5.7.

For HPP, the process efficiency was three times higher at pH 3 than at pH 5.7. These results are in agreement with those of other works in which it was found that under acid medium (normally in the pH range of 2–4) the UV photolysis of H_2O_2 is more efficient in the depletion of dyes than under higher pH [55,56]. When pH rises, H_2O_2 photo-decomposes into H_2O and O_2 rather than $\cdot\text{OH}$ (Eq. (12)) and under alkaline conditions, H_2O_2 dissociates into its conjugated base, the hydroperoxide anion (HO_2^-), and H^+ (Eq. (13)). Then HO_2^- can react with $\cdot\text{OH}$ and residual H_2O_2 (Eqs. (14) and (15)) and, as a result, the discolouration rate is lowered.

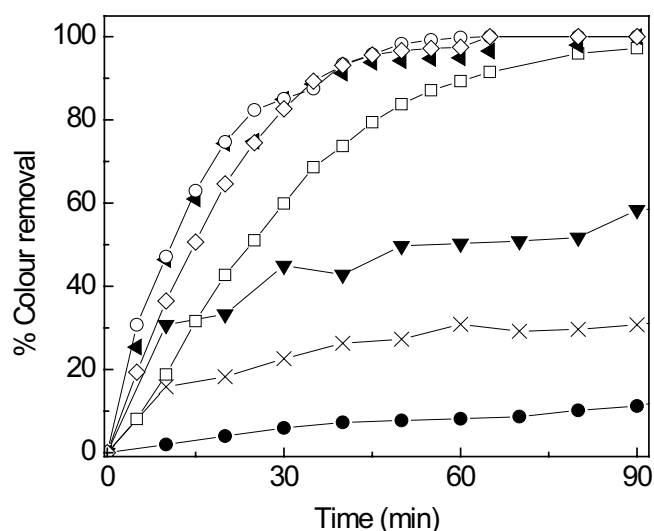
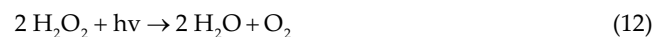


Fig. 5. Percentage of colour removal as function of treatment time through different AOPs. Experimental conditions: $[\text{Ponceau 4R}]_0 = 50 \text{ mg L}^{-1}$, $[\text{H}_2\text{O}_2]_0 = 3.3 \times 10^{-2} \text{ mol L}^{-1}$, $[\text{Catalyst}] = 500 \text{ mg L}^{-1}$, average solar UVA–UVB radiation = 35.4 W m^{-2} , pH = 5.7. Symbols: Adsorption (x), HPP (●), FPF (▼), OZO (◇), PER (□), COZH (◄), PCOH (○).

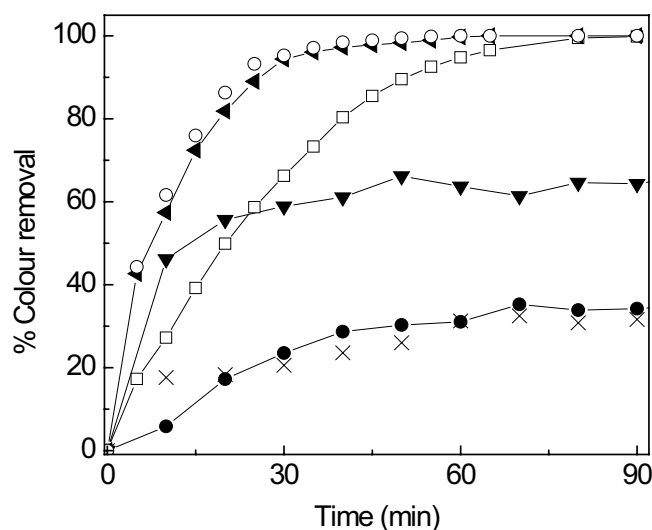


Fig. 6. Percentage of colour removal as function of treatment time through different AOPs. Experimental conditions: $[\text{Ponceau 4R}]_0 = 50 \text{ mg L}^{-1}$, $[\text{H}_2\text{O}_2]_0 = 3.3 \times 10^{-2} \text{ mol L}^{-1}$, $[\text{Catalyst}] = 500 \text{ mg L}^{-1}$, average solar UVA–UVB radiation = 35.4 W m^{-2} , pH = 3. Symbols: Adsorption (x), HPP (●), FPF (▼), PER (□), COZH (◄), PCOH (○).

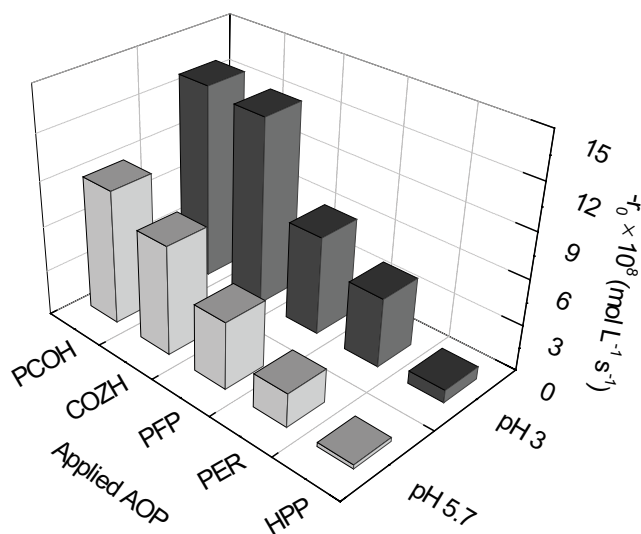
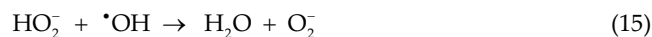
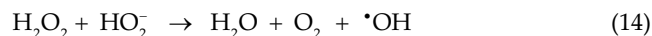
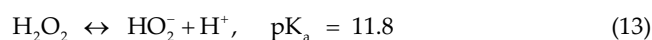


Fig. 7. Initial instantaneous reaction rate for the removal of azo content at pH 3 and 5.7 in some of the applied AOPs. Experimental conditions: [Ponceau 4R]₀ = 50 mg L⁻¹, [H₂O₂]₀ = 3.3 × 10⁻² mol L⁻¹, [Catalyst] = 500 mg L⁻¹, average solar UVA-UVB radiation = 35.4 W m⁻².



It was observed that at pH 3, the HPP system can lead to a similar discolouration yield than that reached by single adsorption.

PFP process was 10% more efficient in colour removal at pH 3 than at natural pH. The initial reaction rate at pH 3 was 6.5 × 10⁻⁸ mol L⁻¹ s⁻¹ and fell to 1.3 × 10⁻⁸ mol L⁻¹ s⁻¹ in 10 min, likely because of the H₂O₂ consumption. Fenton-based processes are known to be less effective at pH values above 3, even in heterogeneous systems. When using solid catalysts, it is thought that H₂O₂, in contact with the iron source (such as hematite or other iron oxide), leads to the formation of Fe²⁺ ions in solution, which in turn undergo homogeneous Fenton reaction in the liquid phase with the remaining H₂O₂. At pH values beyond 3, the dissolved iron ions are poorly soluble affecting the homogeneous H₂O₂ activation [57]. During the application of PFP at pH 3 and 5.7, the exposition to sunlight also led to a rising in the system temperature from ca. 25°C to ca. 38°C, which also affects the system performance. Increasing the temperature in Fenton processes leads to more efficient consumption of H₂O₂ to produce oxidizing radicals [58].

Similar effects were found in COZH and PCOH, for which the initial degradation rates were in average 1.27 × 10⁻⁷ mol L⁻¹ s⁻¹ and the complete colour removal was reached in less than 60 min. The discolouration profile obtained in PCOH was sparsely faster than that of COZH at pH 3.

3.2.4. Kinetic considerations

Eq. (16) describes the degradation rate of an organic compound subjected to a non-photochemical ozone-based AOP as PER. In this equation, the effect of direct oxidation with H₂O₂, O₃ and ·OH is taken into account.

$$\frac{dC_A}{dt} = - \left[k_{\text{H}_2\text{O}_2} \cdot C_{\text{H}_2\text{O}_2} + k_{\text{O}_3} \cdot C_{\text{O}_3} + k_{\cdot\text{OH}} \cdot C_{\cdot\text{OH}} \right] C_A \quad (16)$$

where C_A is the concentration of the pollutant; *t* the reaction time; *k*_{H₂O₂}, *k*_{O₃} and *k*_{·OH} are the kinetic constants for the direct oxidation of the compound with H₂O₂, ozone and ·OH radicals, respectively; and C_{H₂O₂}, C_{O₃} and C_{·OH} are the concentration of H₂O₂, ozone and ·OH radicals, respectively. The experimental data obtained in the PER systems were used to estimate the kinetic rate constant of the direct reaction of ozone with Ponceau 4R using Eq. (16). Since this compound does not undergo direct oxidation with H₂O₂, the value of *k*_{H₂O₂} is zero. Also, as the presence of H₂O₂ exerted a scavenging effect of ·OH radicals, the rate of oxidation with ·OH radicals for this essay can be neglected and consequently, Eq. (16) reduces to:

$$\frac{dC_A}{dt} = - k_{\text{O}_3} \cdot C_{\text{O}_3} \cdot C_A \quad (17)$$

By adjusting Eq. (17) to the experimental data, a value of 77.1 L mol⁻¹ s⁻¹ was obtained for *k*_{O₃} (pH 3–5.7). To the best of our knowledge, no previous estimation of the rate constant of the direct reaction between ozone and Ponceau 4R has been reported. Rate constants for the oxidation of azo dyes by ozone are usually up to 10⁷ L mol⁻¹ s⁻¹ [59,60]. This result falls within this range.

3.2.5. Process efficiency and synergy effect

As in all experiments, the colour decay curve described an exponential pattern with time, they were adjusted to a first order rate law (Eq. (18)). Thus, apparent pseudo-first-order reaction constants were calculated by fitting the experimental data of each oxidation system to a first order kinetics.

$$\frac{dC}{dt} = - k_{\text{app}} \cdot C \quad (18)$$

In Eq. (18), *k*_{app} is the apparent pseudo-first-order reaction constant, *t* is the reaction time and *C* is the concentration of the contaminant.

Then, the efficiency of each process was analyzed in terms of the time required to reach a 99% colour removal (*t*₉₉). Fig. 8 shows the calculated *t*₉₉ for the studied AOPs.

Fig. 8 allows to quickly compare the treatment times that would be required to completely remove the colour from water samples contaminated with Ponceau 4R through the studied systems. PCOH was selected as the reference system as it was the most effective AOP among the ones applied in this work. According to Fig. 8, at pH 3, the application of PER, PFP and HPP would require, respectively, 3-, 10- and

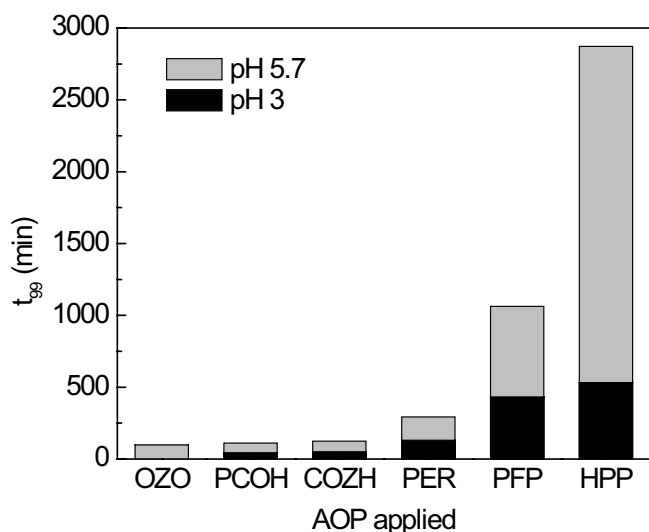


Fig. 8. Theoretical time to complete a 99% conversion of Ponceau 4R for each oxidation experiment. Experimental conditions: $[\text{Ponceau 4R}]_0 = 50 \text{ mg L}^{-1}$, $[\text{H}_2\text{O}_2]_0 = 3.3 \times 10^{-2} \text{ mol L}^{-1}$, $[\text{Catalyst}] = 500 \text{ mg L}^{-1}$, average solar UVA-UVB radiation = 35.4 W m^{-2} .

12-fold the time needed in PCOH treatment to reach 99% contaminant removal. However, to keep the initial reaction rate and avoid the process inactivation, for PER and HPP it would be needed a continuous supply of H_2O_2 . If applied at a pH of 5.7, PCOH would require 50% more of time than that needed at pH 3 to achieve the same degree of colour removal. PER, PFP and HPP at pH 5.7 would require, respectively, 2-, 9- and 35-fold of time compared with PCOH at the same pH. All ozone-based systems, except PER, require very similar reaction times when applied at the same pH. It is noteworthy that COZH and PCOH at pH 5.7 require twice the time compared with pH 3.

These results make evident the synergy effect generated by the application of combined AOPs. Synergy is observed when two processes applied simultaneously produce an effect that is greater than the sum of the individual effects of such processes when implemented separately. That is the case of HPP that led to a 15% of compound depletion, while no degree of elimination was observed by direct oxidation with H_2O_2 or by photolysis in the same reaction time.

3.2.6. Effect of the water matrix

Two samples of surface water were doped with 50 mg L^{-1} of Ponceau 4R to evaluate the removal of this dye through PCOH in these matrices. The samples corresponded to natural seawater (SW) and domestic wastewater (WW) and their characteristics are shown in Table 3.

These experiments were carried out at pH 3 and the natural pH of such water samples (8 and 8.7 for WW and SW, respectively). Fig. 9 shows the results of these essays compared with the ones obtained using deionized water (DW). As a general trend, in DW higher reaction rates are reached compared with SW and WW.

For all matrices, at pH 3 the application of PCOH led to complete colour removal and the initial degradation rates

Table 3
Composition of the used water samples before doping

| Property | Seawater | Domestic wastewater |
|---|--------------|---------------------|
| Chemical oxygen demand (mg L^{-1}) | Undetermined | 212 |
| pH | 8.0 | 8.7 |
| Turbidity (NTU) | 2.24 | 1.02 |
| Conductivity (mS cm^{-1}) | 50 | 0.405 |
| Total solids (mg L^{-1}) | 57,503 | 194 |

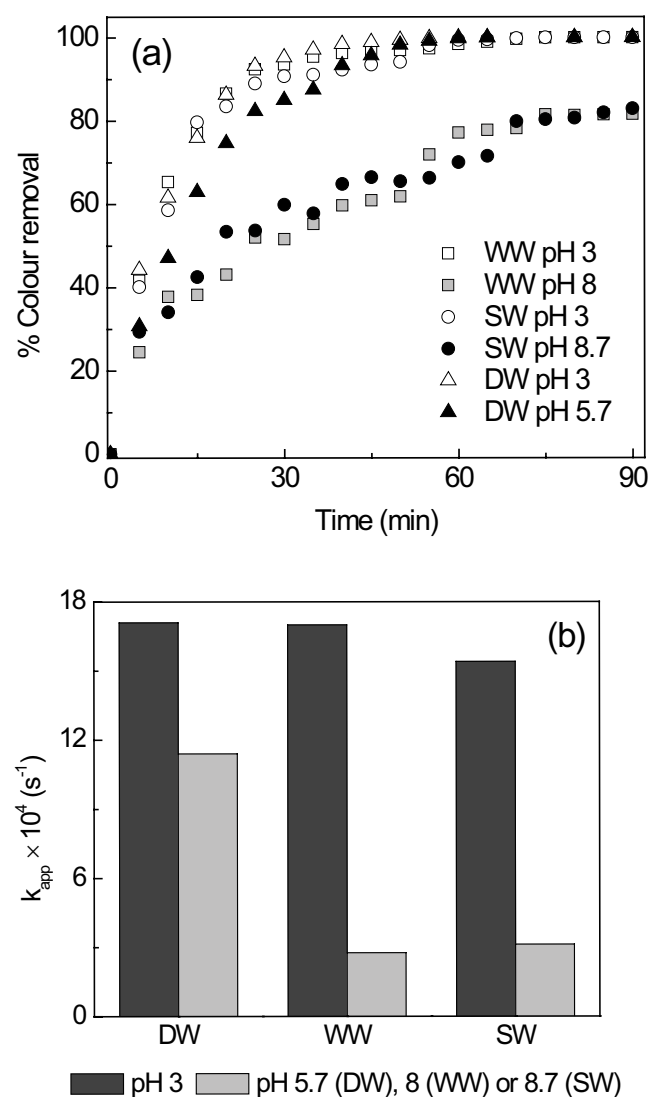


Fig. 9. Percentage of colour removal as function of time (a) and apparent pseudo-first-order reaction constant of the azo group depletion (b) in photocatalytic ozonation treatment (PCOH) for different water matrices doped with Ponceau 4R. Experimental conditions: $[\text{Ponceau 4R}]_0 = 50 \text{ mg L}^{-1}$, $[\text{H}_2\text{O}_2]_0 = 3.3 \times 10^{-2} \text{ mol L}^{-1}$, $[\text{Catalyst}] = 500 \text{ mg L}^{-1}$.

followed the order $DW > SW \approx WW$ (being SW slightly faster than WW). At natural pH, DW led to complete discoloration and for SW and WW the highest removal yields were around 80%. Accordingly, the obtained apparent pseudo-first-order reaction constants were higher at pH 3 than at the matrices' respective natural pH. It is noteworthy that for WW and SW the apparent pseudo-first-order constants diminished, respectively, 84% and 80% at natural pH compared with pH 3.

Spiked Ponceau 4R added an extra theoretical chemical oxygen demand content of 55 mg L^{-1} to the WW, which was equivalent to one fifth of all organic matter present in the sample (expressed as chemical oxygen demand). Given the high concentration of organic compounds in WW, during the treatment Ponceau 4R competed against that organic matter for the generated $\cdot\text{OH}$ radicals to be oxidized, but the oxidation rate for Ponceau 4R was expected to be lower than that of the non-target organic compounds. This slowed down the oxidation rate observed for the target compound in WW compared with DW. Moreover, at the natural pH of the WW the catalyst is negatively charged ($\text{pH} > \text{pH}_{z,c}$) and Ponceau 4R is deionized (see dissociation constants in Table 1). Consequently, at this pH an electrostatic repulsion is developed between the catalyst and the probe molecules. In contrast, when the solution was acidified to reach pH 3, the catalyst surface got positively charged and attracted the pollutant molecules, which still had net negative charge. Lastly, it is known that the acidification of WW significantly reduces its inorganic carbon content which in consequence, diminishes the scavenging effect of the matrix.

Regarding the SW, the high content of salinity, which was evidenced from its conductivity and total solids content, exerted a radical scavenging effect. Ions as Cl^- or H_2PO_4^- may undergo competitive reactions against the target contaminant for the oxidizing species. At alkaline conditions, besides of the negative effect due to the electrostatic repulsion between the catalyst surface and Ponceau 4R molecules, the presence of chloride and other ions precipitates iron ions from the medium by the formation of coordination compounds diminishing the Fenton's reaction efficiency. At acidic conditions, the concentration of iron in solution is expected to be higher since the formation of insoluble iron compounds is reduced [61].

4. Conclusions

Surface water samples (deionized water, domestic wastewater and seawater) containing Ponceau 4R were treated by heterogeneous photocatalytic ozonation and the different sub-processes derived from it (especially, simple ozonation, catalytic ozonation and photocatalytic oxidation). A magnetized activated carbon supported with maghemite and magnetite particles was prepared and used as a Fenton-like catalyst. This catalyst was found to be rich in oxygen-containing groups and easily recoverable from water by a magnetic field. The dye was partially removed by adsorption using the catalyst likely by hydrogen-bonding and π - π stacking interactions. It is also oxidized to some extent by photo-Fenton and UV/hydrogen peroxide oxidation (up to 53%, 64% and 35% respectively, under the following conditions: $[\text{Ponceau 4R}]_0 = 50 \text{ mg L}^{-1}$ in deionized water,

$[\text{H}_2\text{O}_2]_0 = 3.3 \times 10^{-2} \text{ mol L}^{-1}$, $[\text{Catalyst}] = 500 \text{ mg L}^{-1}$, average solar UVA-UVB radiation = 35.4 W m^{-2} and pH 3, which were the best conditions here applied). However, in these reactions the initial depletion rate drastically drops due to the rapid degradation of H_2O_2 in the medium, which suggests that a continuous injection of H_2O_2 would be necessary to maintain the reaction efficiency with time.

The use of ozone was found effective to completely remove the dye within short periods of time (<60 min) when using a deionized water matrix, likely due to the high reactivity of ozone to azo and aromatic groups present in the target compound structure.

In deionized water, COZH (the coupling of heterogeneous Fenton and ozonation) and PCOH (the combination of heterogeneous photo-Fenton and ozonation) led to the highest initial reaction rates, which in average were 12.7×10^8 and $8.0 \times 10^8 \text{ mol L}^{-1} \text{ s}^{-1}$ for pH values of 3 and 5.7, respectively. Very similar efficiency was found when PCOH process was applied in real domestic wastewater and seawater matrices at pH 3; however, when applied at these matrices' natural pH (8 and 8.7, respectively) the process effectiveness was decreased reaching a maximum colour removal yield around 80% after 90 min of treatment. This reduction in the process effectiveness was ascribed to radical scavenging (exerted by the salinity of seawater and non-target organic and inorganic compounds present in wastewater), electrostatic repulsion between the probe molecule and catalyst particles at alkaline conditions, and iron precipitation at high pH values.

Supplementary material

Supplementary material associated with this article is available on the online version at the journal's website.

Acknowledgements

The authors would like to acknowledge the Nanomagnetism Laboratory at Universidad de Los Andes, and the Laboratories of Bioprocesos and Física de los Materiales at Universidad del Atlántico for the characterization analyses. The authors are also grateful to Universidad del Atlántico for the economic support.

References

- [1] K.T. Chung, Azo dyes and human health: a review, *J. Environ. Sci. Health C*, 34 (2016) 233–261.
- [2] P.F. Gordon, P. Gregory, Azo dyes, In: *Organic Chemistry in Colour*, Springer, Berlin Heidelberg, 1987, pp. 95–162.
- [3] J. Smith, L. Hong-Shum, *Food Additives Data Book*, John Wiley & Sons, United Kingdom, 2003.
- [4] K. Bevziuk, A. Chebotarev, D. Snigur, Y. Bazal, M. Fizer, V. Sidey, Spectrophotometric and theoretical studies of the protonation of Allura Red AC and Ponceau 4R, *J. Mol. Struct.*, 1144 (2015) 216–244.
- [5] A.M. Contento, Nuevos métodos fotométricos y cromatográficos para la determinación de colorantes rojos en alimentos, Ediciones de la Universidad de Castilla-La Mancha, Cuenca, 1997.
- [6] EFSA Panel on Food Additives and Nutrient Sources added to Food, Scientific Opinion on the reevaluation of Ponceau 4R (E 124) as a food additive on request from the European Commission, *EFSA J.*, 7 (2009) 1–39.

- [7] S. Tsuda, M. Murakami, N. Matsusaka, K. Kano, K. Taniguchi, Yu F. Sasaki, DNA damage induced by red food dyes orally administered to pregnant and male mice, *Toxicol. Sci.*, 61 (2001) 92–99.
- [8] J. König, Food Colour Additives of Synthetic Origin, In: M.J. Scotter, Colour Additives for Foods and Beverages, Woodhead Publishing, 2015, pp. 35–60.
- [9] National Center for Biotechnology Information, PubChem Compound Database; CID=9570119. Available at: https://pubchem.ncbi.nlm.nih.gov/compound/New_coccine.
- [10] L. Pereira, M. Alves, Dyes—Environmental Impact and Remediation; In: A. Malik, E. Grohmann, Environmental Protection Strategies for Sustainable Development, Springer, New York, 2012, pp. 111–162.
- [11] C. Benincá, P. Peralta-Zamora, C. Regina, G. Tavares, L. Igarashi-Mafra, Degradation of an azo dye (Ponceau 4R) and treatment of wastewater from a food industry by ozonation, *Ozone—Sci. Eng.*, 35 (2013) 295–301.
- [12] Y. Deng, R. Zhao, Advanced oxidation processes (AOPs) in wastewater treatment, *Curr. Pollut. Rep.*, 1 (2015) 167–176.
- [13] J.P. Kehrer, J.D. Robertson, C.V. Smith, Free Radicals and Reactive Oxygen Species, In: C.A. McQueen, Comprehensive Toxicology, 3rd ed., Elsevier, 2018, pp. 262–294.
- [14] S.C. Ameta, Introduction, In: S.C. Ameta, R. Ameta, Advanced Oxidation Processes for Wastewater Treatment, Emerging Green Chemical Technology, 1st ed., Academic Press, 2018, pp. 1–12.
- [15] S. Goldstein, D. Aschengrau, Y. Diamant, J. Rabani, Photolysis of aqueous H_2O_2 : quantum yield and applications for polychromatic UV actinometry in photoreactors, *Environ. Sci. Technol.*, 41 (2007) 7486–7490.
- [16] J.C. Mierzwa, R. Rodrigues, A.C.S.C. Teixeira, UV-Hydrogen Peroxide Processes, In: S.C. Ameta, R. Ameta, Advanced Oxidation Processes for Waste Water Treatment Emerging Green Chemical Technology, 1st ed., Academic Press, 2018, pp. 13–48.
- [17] D. Spuhler, J.A. Rengifo-Herrera, C. Pulgarín, The effect of Fe^{2+} , Fe^{3+} , H_2O_2 and the photo-Fenton reagent at near neutral pH on the solar disinfection (SODIS) at low temperatures of water containing *Escherichia coli* K12, *Appl. Catal., B*, 96 (2010) 126–141.
- [18] G. Cruz-González, C. Julcour, H. Chaumat, U. Jáuregui-Haza, H. Delmas, Degradation of 2,4-dichlorophenoxyacetic acid by photolysis and photo-Fenton oxidation, *J. Environ. Chem. Eng.*, 6 (2018) 874–882.
- [19] D.H. Quiñones, P.M. Álvarez, A. Rey, S. Contreras, F.J. Beltrán, Application of solar photocatalytic ozonation for the degradation of emerging contaminants in water in a pilot plant, *Chem. Eng. J.*, 260 (2015) 399–410.
- [20] J. Herney-Ramirez, M.A. Vicente, L.M. Madeira, Heterogeneous photo-Fenton oxidation with pillared clay-based catalysts for wastewater treatment: a review, *Appl. Catal., B*, 98 (2010) 10–26.
- [21] K. Sivagami, K.P. Sakthivel, I.M. Nambi, Advanced oxidation processes for the treatment of tannery wastewater, *J. Environ. Chem. Eng.*, 6 (2018) 3656–3663.
- [22] M. Aleksić, H. Kušić, N. Koprivanac, D. Leszczynska, A. Lončarić, Heterogeneous Fenton type processes for the degradation of organic dye pollutant in water — The application of zeolite assisted AOPs, *Desalination*, 257 (2010) 22–29.
- [23] J. He, X. Yang, B. Men, D. Wang, Interfacial mechanisms of heterogeneous Fenton reactions catalyzed by iron-based materials: a review, *J. Environ. Sci.*, 39 (2016) 97–109.
- [24] B. Kasprzyk-Hordern, M. Ziótek, J. Nawrocki, Catalytic ozonation and methods of enhancing molecular ozone reactions in water treatment, *Appl. Catal., B*, 46 (2003) 639–669.
- [25] G. Merényi, J. Lind, S. Naumov, C. von Sonntag, Reaction of ozone with hydrogen peroxide (peroxone process): a revision of current mechanistic concepts based on thermokinetic and quantum-chemical considerations, *Environ. Sci. Technol.*, 44 (2010) 3505–3507.
- [26] F. Beduk, M. Emin, A. Ozcan, Degradation of malathion and parathion by ozonation, photolytic ozonation, and heterogeneous catalytic ozonation processes, *Clean Soil Air Water*, 40 (2012) 179–187.
- [27] P.S. Bailey, The reactions of ozone with organic compounds, *Chem. Rev.*, 58 (1958) 925–1010.
- [28] M. Mehrjouei, S. Müller, D. Möller, A review on photocatalytic ozonation used for the treatment of water and wastewater, *Chem. Eng. J.*, 263 (2015) 209–219.
- [29] A.G. Trovó, T.F.S. Silva, O. Gomes, A.E.H. Machado, W. Borges, P.S. Muller, D. Daniel, Degradation of caffeine by photo-Fenton process: optimization of treatment conditions using experimental design, *Chemosphere*, 90 (2013) 170–175.
- [30] Y. Yang, J. Pignatello, J. Ma, W. Mitch, Effect of matrix components on UV/ H_2O_2 and UV/ $S_2O_8^{2-}$ advanced oxidation processes for trace organic degradation in reverse osmosis brines from municipal wastewater reuse facilities, *Water Res.*, 89 (2016) 192–200.
- [31] S. Jiménez, M. Andreozzi, M.M. Micó, M.G. Álvarez, S. Contreras, Produced water treatment by advanced oxidation processes, *Sci. Total Environ.*, 666 (2019) 12–21.
- [32] J. Bacardit, J. Stötzner, E. Chamorro, S. Esplugas, Effect of salinity on the photo-Fenton process, *Ind. Eng. Chem. Res.*, 46 (2007) 7615–7619.
- [33] M. Brumovský, J. Bečanová, J. Kohoutek, M. Borghini, L. Nizzetto, Contaminants of emerging concern in the open sea waters of the Western Mediterranean, *Environ. Pollut.*, 229 (2017) 976–983.
- [34] L. Arpin-Pont, M.J. Martinez, E. Gomez, H. Fenet, Occurrence of PPCPs in the marine environment: a review, *Environ. Sci. Pollut. Res.*, 23 (2016) 4978–4991.
- [35] S. Burgos-Núñez, A. Navarro-Frómata, J. Marrugo-Negrete, G. Enamorado-Montes, I. Urango-Cárdena, Polycyclic aromatic hydrocarbons and heavy metals in the Cispatá Bay, Colombia: A marine tropical ecosystem, *Mar. Pollut. Bull.*, 120 (2017) 379–386.
- [36] M. Fayazi, M.A. Taher, D. Afzali, A. Mostafavi, Enhanced Fenton-like degradation of methylene blue by magnetically activated carbon/hydrogen peroxide with hydroxylamine as Fenton enhancer, *J. Mol. Liq.*, 216 (2016) 781–787.
- [37] S. Laurent, D. Forge, M. Port, A. Roch, C. Robic, L.V. Elst, R.N. Muller, Magnetic iron oxide nanoparticles: synthesis, stabilization, vectorization, physicochemical characterizations, and biological applications, *Chem. Rev.*, 108 (2008) 2064–2110.
- [38] B.M. Babić, S.K. Milonjić, M.J. Polovina, B.V. Kaludierović, Point of zero charge and intrinsic equilibrium constants of activated carbon cloth, *Carbon*, 37 (1999) 477–481.
- [39] W. Masschelein, M. Denis, R. Ledent, Spectrophotometric determination of residual hydrogen peroxide, *Water Sewage Works*, 124 (1977) 69–72.
- [40] E.W. Rice, R.B. Baird, A.D. Eaton, Standard Methods for the Examination of Water and Wastewater, 23rd ed., American Public Health Association, American Water Works Association, Water Pollution Control Federation, New York, 2017.
- [41] W. Kim, C.Y. Suh, S.W. Cho, K.M. Roh, H. Kwon, K. Song, I.J. Shon, A new method for the identification and quantification of magnetite–maghemite mixture using conventional X-ray diffraction technique, *Talanta*, 94 (2012) 348–352.
- [42] A. Sarswat, D. Mohan, Sustainable development of coconut shell activated carbon (CSAC) and a magnetic coconut shell activated carbon (MCSAC) for phenol (2-nitrophenol) removal, *RSC Adv.* 6 (2016) 85390–85410.
- [43] Z.Y. Bai, Q. Yang, J.L. Wang, Fe_3O_4 /multi-walled carbon nanotubes as an efficient catalyst for catalytic ozonation of p-hydroxybenzoic acid, *Int. J. Environ. Sci. Technol.*, 13 (2016) 483–492.
- [44] H. Gupta, R. Kumar, H.S. Park, B.H. Jeon, Photocatalytic efficiency of iron oxide nanoparticles for the degradation of priority pollutant anthracene, *Geosyst. Eng.*, 20 (2017) 21–27.
- [45] D. Beydoun, G.K.C. Low, S. McEvoy, Novel photocatalyst: titania-coated magnetite. Activity and photodissolution, *J. Phys. Chem. B*, 104 (2000) 4387–4396.
- [46] S. Wang, C.W. Ng, W. Wang, Q. Li, Z. Hao, Synergistic and competitive adsorption of organic dyes on multiwalled carbon nanotubes, *Chem. Eng. J.*, 197 (2012) 34–40.

- [47] L.R. Radovic, I.F. Silva, J.I. Ume, J.A. Menéndez, C.A.L.Y. Leon, A.W. Scaroni, An experimental and theoretical study of the adsorption of aromatics possessing electron-withdrawing and electron-donating functional groups by chemically modified activated carbons, *Carbon*, 35 (1997) 1339–1348.
- [48] A.S. Özen, P. Doruker, V. Aviyente, Effect of cooperative hydrogen bonding in azo-hydrazone tautomerism of azo dyes, *J. Phys. Chem. A*, 111 (2007) 13506–13514.
- [49] A. Lopez, H. Benbelkacem, J.S. Pic, H. Oxidation pathways for ozonation of azo dyes in a semi-batch reactor: a kinetic parameters approach, *Environ. Technol.*, 25 (2004) 311–321.
- [50] M. Matsui, Y. Iwata, T. Kato, K. Shibata, Reaction of aromatic azo compounds with ozone, *Dyes Pigm.*, 9 (1988) 109–117.
- [51] C.H. Kuo, L. Zhong, M.E. Zappi, A.P. Hong, Kinetics and mechanism of the reaction between ozone and hydrogen peroxide in aqueous solutions, *Can. J. Chem. Eng.*, 77 (1999) 473–482.
- [52] K. Sharma, R.K. Vyas, K. Singh, A.K. Dalai, Degradation of a synthetic binary dye mixture using reactive adsorption: experimental and modeling studies, *J. Environ. Chem. Eng.*, 6 (2018) 5732–5743.
- [53] H. Valdes, C.A. Zaror, Heterogeneous and homogeneous catalytic ozonation of benzothiazole promoted by activated carbon: kinetic approach, *Chemosphere*, 65 (2006) 1131–1136.
- [54] J. Rivera-Utrilla, M. Sánchez-Polo, Ozonation of 1,3,6-naphthalenetrisulphonic acid catalysed by activated carbon in aqueous phase, *Appl. Catal., B*, 39 (2002) 319–329.
- [55] M. Muruganandham, M. Swaminathan, Photochemical oxidation of reactive azo dye with UV-H₂O₂ process, *Dyes Pigm.*, 62 (2004) 269–275.
- [56] C. Galindo, A. Kalt, UV-H₂O₂ oxidation of monoazo dyes in aqueous media: a kinetic study, *Dyes Pigm.*, 40 (1998) 27–35.
- [57] A.L. Pham, C. Lee, F.M. Doyle, D.L. Sedlak, A silica-supported iron oxide catalyst capable of activating hydrogen peroxide at neutral pH values, *Environ. Sci. Technol.*, 43 (2009) 8930–8935.
- [58] J.A. Zazo, G. Pliego, S. Blasco, J.A. Casas, J.J. Rodriguez, Intensification of the Fenton process by increasing the temperature, *Ind. Eng. Chem. Res.*, 50 (2011) 866–870.
- [59] A.C. Gomesa, J.C. Nunesa, R.M.S. Simões, Determination of fast ozone oxidation rate for textile dyes by using a continuous quench-flow system, *J. Hazard. Mater.*, 178 (2010) 57–65.
- [60] F.J. Beltrán, P. Álvarez, Rate constant determination of ozone-organic fast reactions in water using an agitated cell, *J. Environ. Sci. Health A*, 31 (1996) 1159–1178.
- [61] R. Maciel, G.L. Sant'Anna, M. Dezotti, Phenol removal from high salinity effluents using Fenton's reagent and photo-Fenton reactions, *Chemosphere*, 57 (2004) 711–719.

Supplementary information

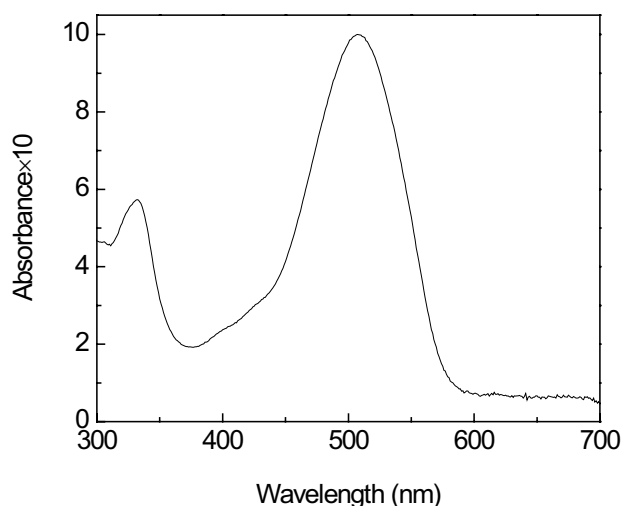


Fig. S1. Ponceau 4R UV-visible absorption spectra.

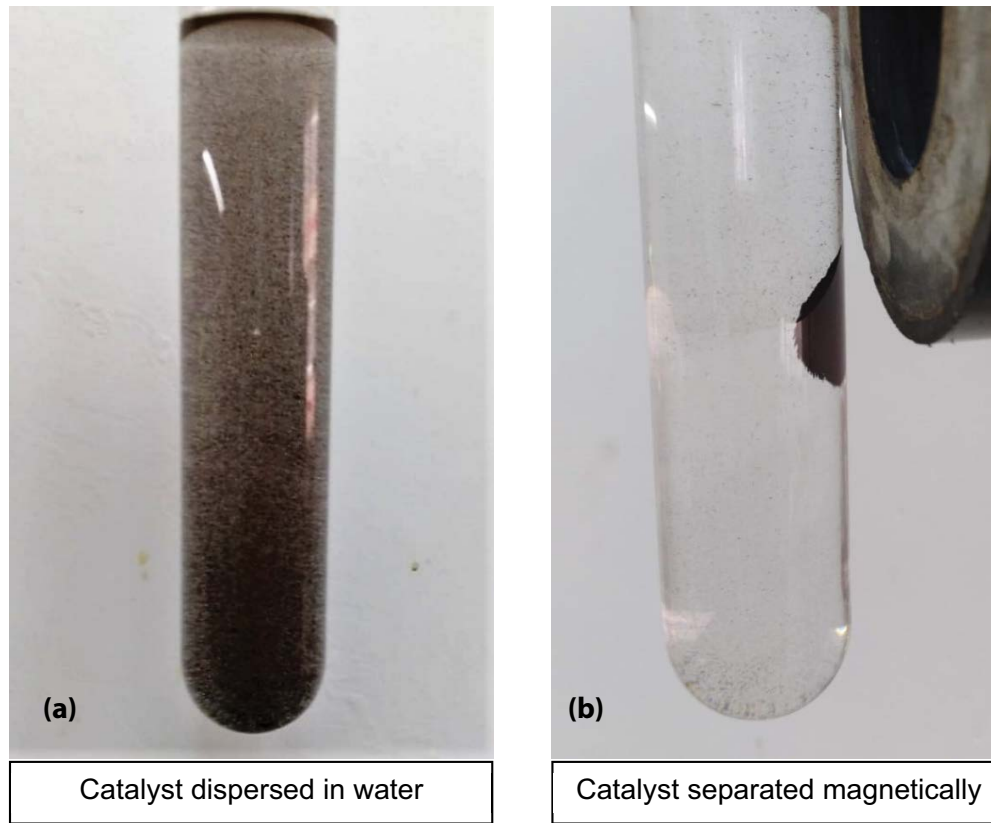


Fig. S2. Photographs of the catalyst dispersed in water (a) and separated by the effect of a magnet placed near to the system (b).

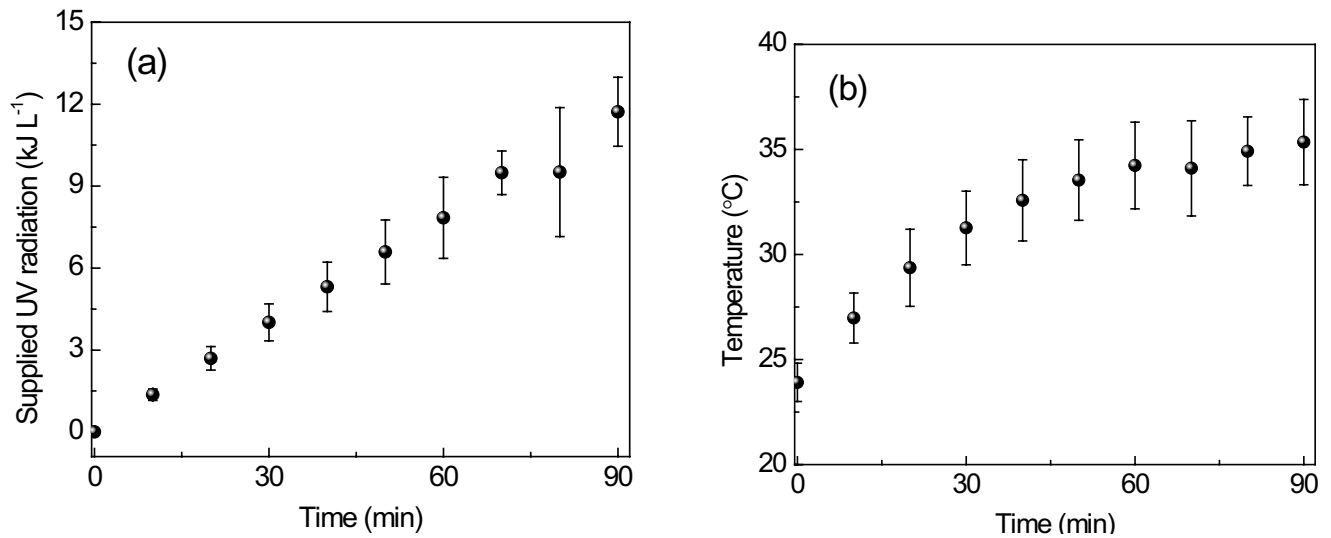


Fig. S3. Evolution of average (a) total UV radiation supplied to the system and (b) system temperature evolution during the sunlight-mediated AOPs applied in this work.

The supplied UV radiation to the system, $Q_{UV,n}$ was computed using Eq. (S1):

$$Q_{UV,n} = Q_{UV,n-1} + (t_n - t_{n-1}) \cdot I_n \cdot \frac{S}{V} \tag{S1}$$

where t_n is elapsed irradiation time until sample n , I_n is the average incident UVA and UVB radiation in the period $t_{n-1} - t_n$, S is the irradiated surface and V is the total reaction volume.

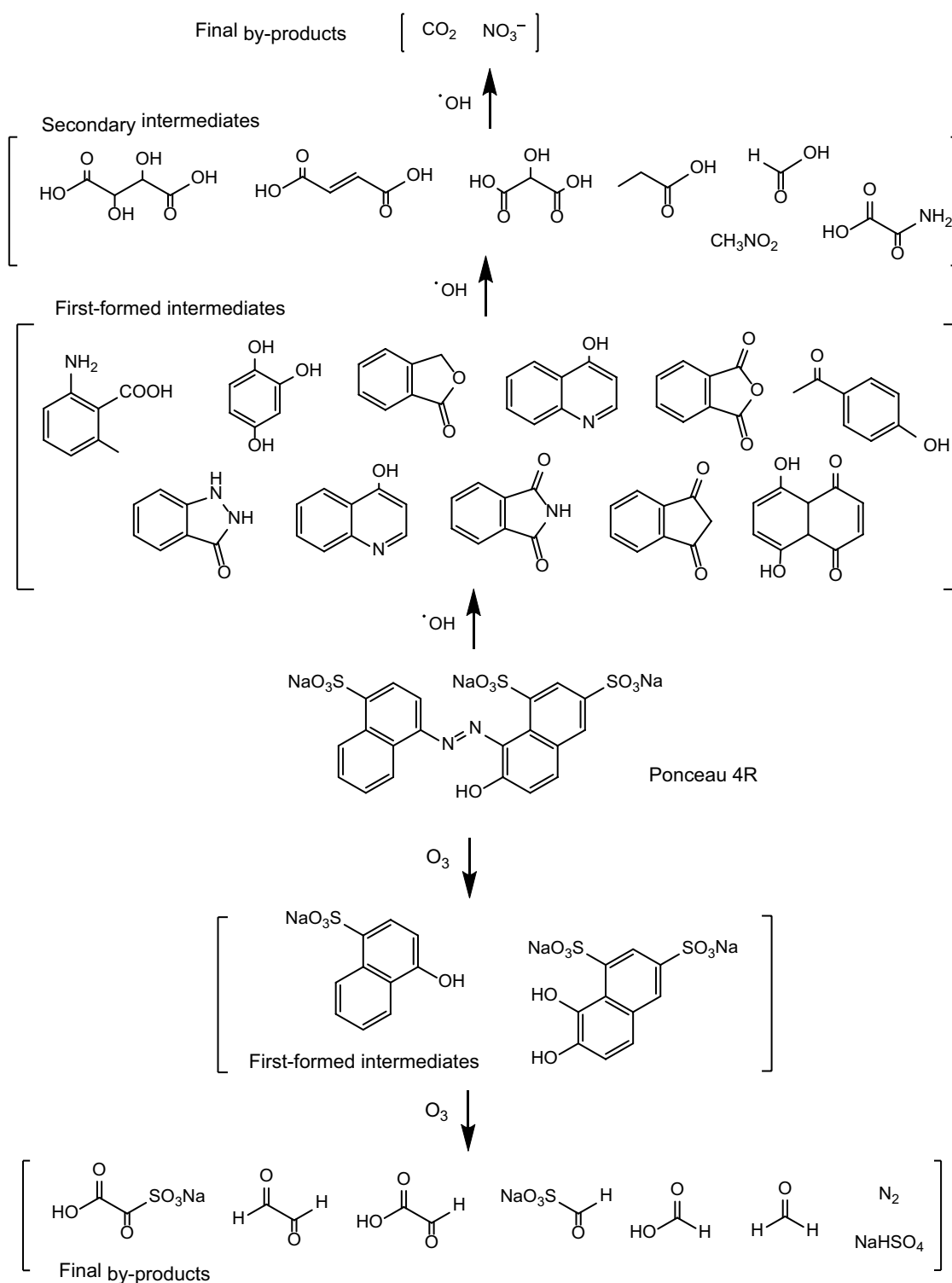


Fig. S4. Proposed simplified mechanism for the degradation of Ponceau 4R by attack of $\cdot\text{OH}$ or O_3 based on the results of some preceding works [S1–S3].

References

- [S1] A. Thiam, E. Brillas, J.A. Garrido, R.M. Rodríguez, I. Sirés, Routes for the electrochemical degradation of the artificial food azo-colour Ponceau 4R by advanced oxidation processes, *Appl. Catal., B*, 180 (2016) 227–236.
- [S2] A. Demirev, V. Nenov, Ozonation of Two Acidic Azo Dyes with Different Substituents, *Ozone–Sci. Eng.*, 27 (2005) 475–485.
- [S3] C. Tizaoui, N. Grima, Kinetics of the ozone oxidation of Reactive Orange 16 azo-dye in aqueous solution, *Chem. Eng. J.*, 173 (2011) 463–473.